Lattice vibrations and phonon-plasmon coupling in Raman spectra of p-type $In_{0.53}Ga_{0.47}As$

A. M. Mintairov
A. F. Ioffe Physical-Technical Institute RAS, 194021, Politechnicheskaya 26, St. Petersburg, Russia

H. Temkin
Electrical Engineering Department, Texas Tech University, Lubbock, Texas 794009
(Received 27 September 1996)

Raman spectra of p-type $In_{0.53}Ga_{0.47}As$ with doping levels ranging from $p=2\times10^{17}$ to 5×10^{19} cm^{-3} have been investigated. Analysis of the Raman line shape and its dependence on the free-hole density demonstrates four-mode behavior of optical phonons. Based on the oscillator strength and Faust-Henry factors of the optical phonons determined from the Raman data, and lattice-dynamic calculations of the phonon dispersion relations in ordered structures of $InGaAs_2$, we show a relationship between the observed four-mode behavior and short-range order phase-separation effects. [S0163-1829(97)10807-4]

I. INTRODUCTION

In piezoelectric cubic semiconductors longitudinal components of polar optic (dipole active) vibrations interact with plasma vibrations of free carriers created by donor or acceptor doping.[1] These vibrations are strongly coupled when the plasma frequency (ω_e) is close to the frequency of longitudinal optical phonons (ω_{LO}) leading to a strong dependence of the infrared dielectric function on free carrier density. At high doping levels, when $\omega_e \gg \omega_{LO}$, the electric field responsible for the longitudinal-transverse splitting of the optical vibrations is completely screened. In other words, neglecting local field effects,[2] the frequency of screened longitudinal optical (LO) phonons is the same as that of transverse (TO) ones. The coupled modes are called phonon-plasmon modes (PPM). They can be observed directly in Raman scattering spectra of doped semiconductors.[13]

Raman spectra (RS) from PPM have been studied in detail in binary zinc-blende semiconductors having a single dipole active phonon.[4] It is well established that RS from PPM strongly depend on the plasmon damping, light scattering mechanisms, and the scattering wave vector. Such spectra provide information about the dependence of the free-electron gas susceptibility on the frequency and wave vector and can be used for measurements of density and mobility of free carriers.

Novel aspects of phonon-plasmon coupling arise in ternary and multinary semiconductor alloys. Here, the spectrum of the dipole active vibrations becomes more complicated due to disorder,[5] phase separation, and spontaneous ordering[6–8] effects. Investigation of the RS dependence on free-carrier density allows for identification of the longitudinal and transverse components of the dipole active vibrations, which in turn permits identification of specific lattice distortion effects.[7] However, while the experimental spectra of a variety of III-V semiconductor alloys with varying doping, n-$Al_xGa_{1-x}As$ ($x=0.1$–0.3) (Refs. 9–13) and ($x=0.5$–0.8) (Ref. 14), p-$Al_{0.2}Ga_{0.8}As$,[15] n-$In_{0.2}Ga_{0.8}As$,[16] p-$In_{0.3}Ga_{0.7}As$,[17] n-$Ga_{0.5}In_{0.5}P$,[18] have been investigated, the PPM Raman line-shape analysis and identification of the dipole active vibrations have been performed only in a few cases, such as n-type $Al_xGa_{1-x}As$ ($x=0.1$–0.9) (Refs. 13 and 14) and relaxed $In_{0.2}Ga_{0.8}As$ (Ref. 16) grown on GaAs. The PPM Raman line shape of lattice-matched $Al_xGa_{1-x}As$ could be described by a two-mode model, while a three-mode model was used for lattice-mismatched $In_{0.2}Ga_{0.8}As$. The additional dipole active mode in the phonon spectra of $In_{0.2}Ga_{0.8}As$ was identified as the vibration of a partially ordered phase of $InGaAs_2$.[7]

The alloy of $In_{0.53}Ga_{0.47}As$, lattice matched to InP, is well suited for the investigation of the relationship between the microstructure and lattice vibrations. Phase separation effects in this alloy, widely used for optoelectronic devices,[19] are well documented.[20] Transmission electron microscopy of epitaxial layers grown on (001) substrates shows a fine-scale speckle microstructure aligned along the [100] and [010] directions. The period of modulation varies from 5 to 10 nm, depending on the growth technique and conditions. It is assumed that the modulation results from variations, on the order of a few percent, in the average alloy composition.

Raman scattering of undoped $In_{0.52}Ga_{0.47}As$ has been investigated previously and the spectra from (001), (110), and (111) surfaces have been reported.[21–26] In the spectral range of 200–300 cm^{-1} the RS consist of several overlapping bands. The identification of the bands was done in terms of two-mode behavior of optical phonons.[27–29] That is, the InAs and GaAs-type longitudinal (LO) and transverse (TO) optical phonons have been identified in the spectra. An additional band, at 244 cm^{-1}, which did not fit the two-mode behavior, was also observed. The presence of this band was attributed to alloy disordering.

The goal of our study of RS of p-type $In_{0.53}Ga_{0.47}As$ is to identify the dipole-active optical modes and to establish a correlation between the phonon spectra and phase-separation effects. The RS dependence on free-carrier density, together with molecular model[7] calculations of the Raman line shape, is used to separate out the longitudinal and transverse components of optical vibrations in $In_{0.53}Ga_{0.47}As$. Our analysis shows a four-mode behavior of lattice vibrations of $In_{0.53}Ga_{0.47}As$. The oscillator strengths and Faust-Henry factors of $In_{0.53}Ga_{0.47}As$ optical phonons are determined from the RS. The alloy lattice vibrations are analyzed from the

TABLE I. Parameters of p-$In_{0.53}Ga_{0.47}As$ samples.

Sample identification	Free-hole density (10^{+17} cm^{-3})	
	Hall	Raman[a]
$N1$	2.6	
$N2$	12	8 (50)
$N3$	100	200 (900)
$N4$	500	500 (350)

[a]Values of the plasma damping constants (in cm^{-1}) are given in parentheses.

point of view of the lattice dynamics of the simplest ordered structures of $InGaAs_2$. The possibility of a relationship between the observed four-mode behavior and phase separation together with short-range order effects is discussed.

II. RAMAN LINE SHAPE

The samples were grown by metalorganic molecular-beam epitaxy on (100)-oriented InP substrates and doped with Be.[30] The doping levels varied from $p=2\times10^{17}$ to 5×10^{19} cm^{-3}, as determined by Hall measurements. The sample parameters are listed in Table I. The In content was measured by x-ray diffraction. Room-temperature Raman spectra were obtained with a 2.41-eV argon laser line excitation. Backscattering geometry in the $z(xy)z^-$ polarization was used, where x,y,z correspond to [100], [010], and [001] crystallographic directions, respectively. In this polarization Raman scattering from LO phonons and PPM is determined by the deformation potential and the electro-optic effect.[4,31,32] The exciting light penetration depth for $In_{0.53}Ga_{0.47}As$ is equal to $\alpha^{-1}\sim40$ nm, where α is the absorption coefficient.[33] On the other hand, the surface depletion layer is estimated to be $d_{\rm dep}[\rm nm]\sim2.2\times10^{10}/(p[\rm cm^{-3}])^{0.5}$. Thus for $d_{\rm dep}<\alpha^{-1}$, which corresponds to $p>2.5\times10^{17}$ cm^{-3}, the Raman spectra contain PPM contributions from the bulk and unscreened LO phonons from the surface depletion layer. Lorentzian contour modeling is used to distinguish between these contributions.

The Raman line shape was analyzed using a molecular model of the electronic polarizability of the zinc-blende structure alloy.[7] In this model, the frequency dependence of the scattering efficiency for a dipole-allowed Stokes component of the Raman spectrum of a multimode alloy is given by

$$I(\omega)=A(\omega,T)(d_E)^2\mathrm{Im}\left\{-\varepsilon(\omega,q)^{-1}\left(1+\sum_j K_j\chi_j(\omega)\right)^2+\sum_j (K_j)^2\chi_j(\omega)\right\}, \tag{1}$$

where $A(\omega,T)$ includes terms that account for the scattering and collection geometries and the propagation conditions for the exciting and scattered light in the crystal, and the temperature. The quantity $\varepsilon(\omega,q)=\varepsilon_\infty+\Sigma_j\chi_j(\omega)+\chi_e(\omega,q)$ is the low-frequency dielectric constant of the crystal, where ε_∞, $\chi_j(\omega)$, and $\chi_e(\omega,q)$ are the susceptibilities of the bound electrons, phonons (where j specifies the optical phonon type), and free carriers (where q is the wave vector), respectively. In the coefficient $K_j=C_jS_j^{-1}$, S_j is the oscillator strength, and C_j is the Faust-Henry coefficient normalized to the total number of bonds. The factor C_j is proportional to the ratio of the deformation potential (d_{Qj})and electro-optic (d_E) contributions to the electronic polarizability of the crystal.

The phonon susceptibilities are calculated from

$$\chi_j=S_j(\omega_{\rm TOj})^2[(\omega_{\rm TOj})^2-\omega^2-i\omega\gamma_j]^{-1},$$
$$S_j=\prod_{k\neq j}[(\omega_{\rm LOk})^2-(\omega_{\rm TOj})^2][(\omega_{\rm TOk})^2-(\omega_{\rm TOj})^2]^{-1}(\omega_{\rm TOj})^{-2}, \tag{2}$$

were $\omega_{\rm TOj}$ ($\omega_{\rm LOj}$) is the frequency of the transverse (longitudinal) optical phonon and γ_j is the phonon damping constant.

The expression for the free-hole susceptibility of a zinc-blende semiconductor contains three contributions from intra- and inter-valence-band transitions within the light- and heavy-hole bands. In the calculation of the plasmon susceptibility we account only for the contribution of the intraband heavy-hole transitions. This is justified by the low density of light holes. Good fits to the PPM line shape can be obtained with this assumption.[34] The intraband heavy-hole contribution was calculated using an expression[35] based on a hydrodynamic model:

$$\chi_e(\omega,q)=-\omega_e^2(\omega^2-3/5\nu_Fq-i\omega\gamma_e)^{-1}, \tag{3}$$

where the plasma frequency $\omega_e^2=(4\pi ep)/(\varepsilon_\infty m_{\rm hh})$, p is the free-hole density, $m_{\rm hh}$ is the heavy-hole effective mass; γ_e is the plasmon damping, e, ν_F, and q are the electron charge, Fermi velocity of holes, and the scattering wave vector, respectively.

The screening of the longitudinal-transverse (LO-TO) splitting for $\omega_e\gg\omega_{\rm LOj}$ follows from expression (1). Here, for $\omega_e\gg\omega_{\rm LOj}$ and $\omega\sim\omega_{\rm LOj}$, one can neglect the first term in curly brackets. The remaining terms describe the scattering from TO phonons under backscattering conditions.[7] The optical constants in $A(\omega,T)$ the electro-optic component of the electron polarizability (d_E), and the high-frequency dielectric constant (ε_∞) of $In_xGa_{1-x}As$ used in calculating the Raman spectrum are obtained by linear interpolation of the corresponding values for GaAs and InAs (virtual-crystal approximation), which have been determined previously.[33,36] We determine the numerical value of the normalization factor $A(\omega,T)$ by fitting the Raman spectrum of GaAs [$C^0_{\rm GaAs}=-0.55$ (Ref. 37)], which was measured under the same conditions. The details of this procedure have been described previously.[7]

The frequencies and damping constants of the optical phonons, which determined χ_j, were estimated from experimental spectra (see Table II). The free-hole density and plasmon damping values were obtained by fitting the calculated PPM Raman line shape to the experimental data. They are listed in Table I.

The experimental Raman spectra and the calculated line shapes for the four samples investigated here (see Table I) are shown in Figs. 1(a)–1(d). The PPM are labeled L_j, where the subscript j is the same as in expression (1).

In Fig. 1(b) (sample $N2$, $p=10^{18}$ cm^{-3}) we show the contour labeled L_P (dotted line with a maximum at 270

TABLE II. Parameters of optical phonons of $In_{0.53}Ga_{0.47}As$ obtained from Raman spectra. Heavy-hole effective mass m_{hh} is 0.5 (Ref. 20).

Phonon type	GaAs type		InAs type	
Primitive cell (phase)	*A*	*B*	*A*	*B*
Transverse frequency ω_{TOj} (cm^{-1})	260	250	240	225
Longitudinal frequency ω_{LOj} (cm^{-1})	268	255	242	230
Damping γ_j (cm^{-1})	2(15)**	15	15	15
Oscillator strength S_j;	0.28	0.55	0.27	0.88
effective charge e_j^{0} [b]	1.68	2.4	1.71	2.72
Faust-Henry factor (a)C_j	−0.08	−0.12	−0.1	−0.3
(b) C_j^{0} [b]	−0.47	−0.79	−0.31	−0.84
Effective charge of binaries	2.2		2.53	
Faust-Henry factor of binaries	−0.55			

[a]Values used in calculation of the phonon-plasmon spectra for samples $N2-N4$ are given in brackets.

[b]Values normalized to the number of bonds of a given type.

cm^{-1}). It corresponds to the PPM contribution obtained from Lorentzian contour modeling. It is used to fit the corresponding part of the calculated PPM line shape (solid line). Our analysis shows that in the frequency range of 200–300 cm^{-1} $In_{0.53}Ga_{0.47}As$ has four types of optical phonons interacting with free-hole plasma vibrations. We denote these phonons by subscripts jA and jB and use $j=1$ and $j=2$ to denote GaAs- and InAs-type vibrations, respectively. We assume that the lattice of $In_{0.53}Ga_{0.47}As$ has two types of local atomic arrangements (phases), *A* and *B*, and that each phase has one GaAs- and one InAs-type polar optical vibration.

The spectra of samples $N1$ and $N2$ [$p=2.6\times10^{17}$ and 10^{18} cm^{-3}, Figs. 1(a) and 1(b)] are similar. They consist of a sharp intense line of the LO_{1A} phonon at 268 cm^{-1} and three weak broad overlapping bands, LO_{1B}, LO_{2B}, and LO_{2A}, in the frequency range of 230–260 cm^{-1}. The peaks of the LO_{2B} band are clearly resolved, at 233 cm^{-1}, while those of the LO_{2A} and LO_{1B} bands at 242 and 255 cm^{-1}, not seen in the spectra, must be separated by Lorentzian contour modeling.[6] The intensity of the LO_{1A} phonon line is slightly lower and its half-width is larger for sample $N2$, as compared with sample $N1$.

The intensity distribution changes considerably for samples $N3$ and $N4$ [$p=10^{19}$ and 5×10^{19} cm^{-3}, Figs. 1(c) and 1(d)]. This is due to the strong decrease in the LO_{1A} phonon line intensity and the appearance of a new L_{2B} band at the low-frequency side of LO_{2B}. In sample $N3$ the L_2 band has the same intensity as the LO_{2B} band in samples $N1$ and $N2$. We can also see the appearance of new features in the spectra. They are the weak low-frequency shoulder L_{1A} at 262 cm^{-1} and a long tail on the high-frequency side of the LO_{1A} line. In sample $N4$, the shoulder L_{1A} and the high-frequency tail disappear and clear maxima L_{1B} and L_{2A} become resolved at 240 and 252 cm^{-1}. At the same time, the frequency of the L_{2B} and L_{2A} become resolved at 240 and 252 cm^{-1}. At the same time, the frequency of the L_{2B} maximum band shifts to 225 cm^{-1} and its intensity doubles. Thus

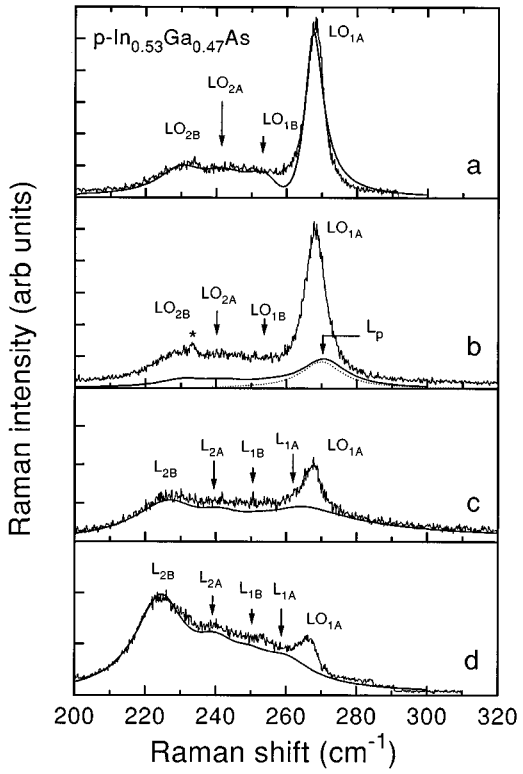

FIG. 1. Experimental and calculated Raman spectra of *p*-type $In_{0.53}Ga_{0.47}As$. The doping levels are (a) 2.6×10^{17}, (b) 1.2×10^{18}, (c) 1×10^{19}, and (d) 5×10^{19} cm^{-3}. The spectra were measured in backscattering (xy) polarization with a 514.5-nm Ar-laser line excitation at 300 K. The dashed curve in (b) is the PPM contribution to the spectrum obtained by Lorentzian contour modeling. The arrows indicate band maxima obtained from RS line shape modeling. The asterisk marks a plasma discharge line.

the overall RS shape of sample $N4$ is characterized by decreasing intensity with increasing frequency.

It is clear that the changes in the Raman line shape in the spectra shown in Figs. 1(a)–1(d) are due to interactions of the LO components of lattice vibrations of $In_{0.53}Ga_{0.47}As$ with the plasma vibrations of free holes. The contribution of PPM modes in samples $N1$ and $N2$ is quite small because of the conditions $d_{depl}\sim\alpha^{-1}$ and $\omega_{LOp}\gg\omega_c$. This contribution is seen only in the spectrum of $N2$ [Fig. 1(b)] as a broadening of the LO_{1A} band. After accounting for the contribution of the unscreened LO phonons from the surface depletion layer, the calculated PPM Raman line shape for samples $N2-N4$ are in good agreement with experimental spectra. The deep minimum, at 260 cm^{-1}, in the calculated Raman line shape of sample $N1$ [Fig. 1(a)], as well as a low value of the LO_{1A} damping constant (2 cm^{-1}), are due to interference effects.[13] These features could be possibly eliminated by accounting for the frequency dispersion of the model oscillators, i.e., nonhomogeneous broadening.

The values of free-hole concentrations used in the fits are in good agreement with the carrier concentrations determined by Hall measurements. For sample $N4$, we satisfy the condition of full screening of the LO-TO splitting, i.e., $\omega_e\gg\omega_{LO}$. The intensity distribution of the RS for this sample coincides with that obtained previously for TO phonons in $In_{0.53}Ga_{0.47}As$.[26]

The oscillator strengths (OS) and Faust-Henry factors (FHF) obtained for the four optical modes of $In_{0.53}Ga_{0.47}As$ are given in Table II. These values are normalized to the total number of bonds and thus include a factor equal to the relative content of bonds contributing to a given phonon. The values of OS and FHF for the Aj phonons are considerably lower than those for the Bj type, which indicates a lower content of the A phase. The notations A and B, as defined above, refer to two types of possible local atomic arrangements, each of which has one GaAs- and one InAs-type polar optical vibration. The frequencies of the Aj-type phonons are higher than those of Bj.

Table II presents effective charges (e_j^0) and FHF (C_j^0) normalized to the number of bonds contributing to a given phonon. These values have been calculated assuming that the A and B phases correspond to an average alloy composition $x \sim 0.5$; i.e., the crystal can be described by a structural formula of $InGaAs_2$ and $x_A = x_B$, where x_A (x_B) is the content of phase A (B). The fitted values are close to the corresponding values for the binary compounds, also given in Table II, thus confirming the $InGaAs_2$ formula for both phases. For further analysis we need to determine the specific type of atomic arrangement, i.e., the cluster type for A and B phases. This will be done in the following section, using the transmission electron microscopy (TEM) data[20] and the lattice dynamics calculations for III-V compounds.

III. DISCUSSION

The simplest choice of clusters characterizing the multimode behavior of optical vibrations in the ternary III-V semiconductor alloys is that proposed by Verleur-Barker (VB).[38] They described lattice vibrations of an $A_xB_{1-x}C$ alloy by the internal vibrations of five weakly coupled molecular complexes (elementary tetrahedrons) $A_nB_{4-n}C$ (where $n=0$–4). This description leads to eight optical modes, four of which are the vibrations of A-C bonds and four are of B-C bonds, in different types of molecular complexes. This model has been used to estimate the relative content of different elementary tetrahedrons in $GaAs_xP_{1-x}$ (Ref. 38) and $In_xGa_{1-x}As$ (Ref. 27). In both of these studies, the application of the VB model gave an excess of A_4C and B_4C tetrahedrons as opposed to a random distribution, i.e., a strong short-range order (SRO) effect of the clustering type. This result, however, is in contradiction with all theoretical models of the SRO in III-V alloys, which predict anticlustering (i.e., an excess of A_3BC, A_2B_2C, and AB_3C tetrahedrons) for alloys of binaries with dissimilar bond lengths.[6] Our analysis shows that the prediction of clustering arises in the VB model from the following relation between the nearest-neighbor force constants: $k_1(1)<k_1(2)<k_1(3)<k_1(4)$ (in the notation of VB), where the subscript 1 is associated with the BC bond and the numbers in parentheses correspond to $n+1$ in the structural formula of a tetrahedron, i.e., $k_1(1) = k_{BC}(B_4C)$, $k_1(2)=k_{BC}(AB_3C)$, etc. The same relation was chosen for A-C bonds. Such a choice of force constants, however, is not consistent with the lattice dynamics of III-V compounds. Indeed, these VB force constant relations imply that the phonon frequencies of the BC binary zinc-blende compounds should be lower than the frequencies of the BC-type phonons of perfectly ordered ternaries, i.e., $\omega_{BC}(B_4C) < \omega_{BC}(AB_3C)$, etc. The phonon frequencies of the ordered ternaries can be deduced from the folding of the zinc-blende phonon zone, having negative dispersion, and the relative magnitudes of the frequencies must be reversed.

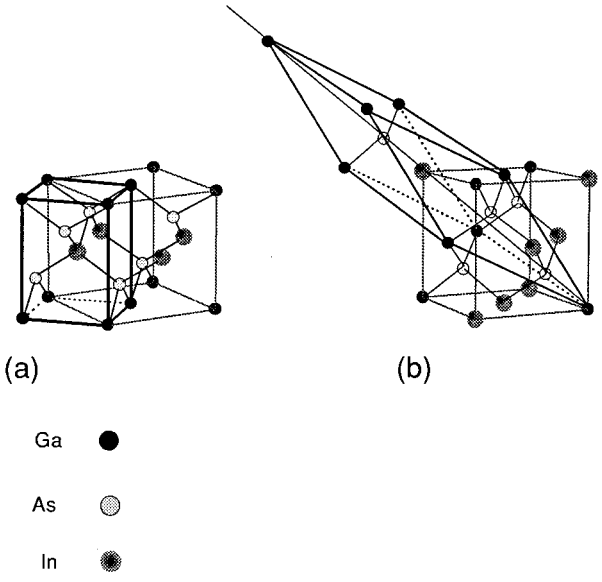

FIG. 2. Schematic drawings illustrating symmetrical cells of CuAu and CuPt-type $InGaAs_2$ ordered structures in a zinc-blende lattice.

It can be shown that for the appropriate choice of the force constants, i.e., $k_1(1)>k_1(2)>k_1(3)>k_1(4)$, the VB model yields anticlustering, in agreement with theoretical predictions. However, in spite of the fact that the VB model can correctly predict the SRO effects, it does not account for the anisotropy of the short-range forces or phase-separation effects. Moreover, due to a strong long-range Coulomb contribution to interatomic forces, the description of polar optical vibration in III-V alloys by a set of strongly localized vibrations of the simplest molecular complexes $A_nB_{n-4}C$ is questionable.

A different description can be formulated on the basis of detailed analysis of TEM results. It is well known that the bonds of binary constituents of III-V alloys are ''relaxed,'' i.e., the alloy values of the bond lengths are close to those of pure binaries.[39] The atoms of an alloy lattice are thus shifted from their exact zinc-blende positions. This means that each elementary tetrahedron may be deformed along some crystallographic axis but lattice matched in some other direction. The directions of the deformation are different for different types of tetrahedrons. For $n=0,2,4$ strains occur along the {001} and {110} directions, and along the {111} and {110} directions for $n=1,3$. Experimentally, plane view TEM micrographs show that phase separation, and thus the principal strain in the (001)-oriented $In_{0.53}Ga_{0.47}As$ layers, lies in the growth planes along the [100] and [010] directions.[20] Cross-sectional TEM data are available only for $In_{1-x}Ga_xAs_yP_{1-y}$, which shows phase-separation effects similar to those of $In_{0.53}Ga_{0.47}As$. In the images of the (110) cross section fine-scale modulation is observed for the (-220) operating reflections. The modulation contrast is not observed for the (004) reflection. The absence of modulation

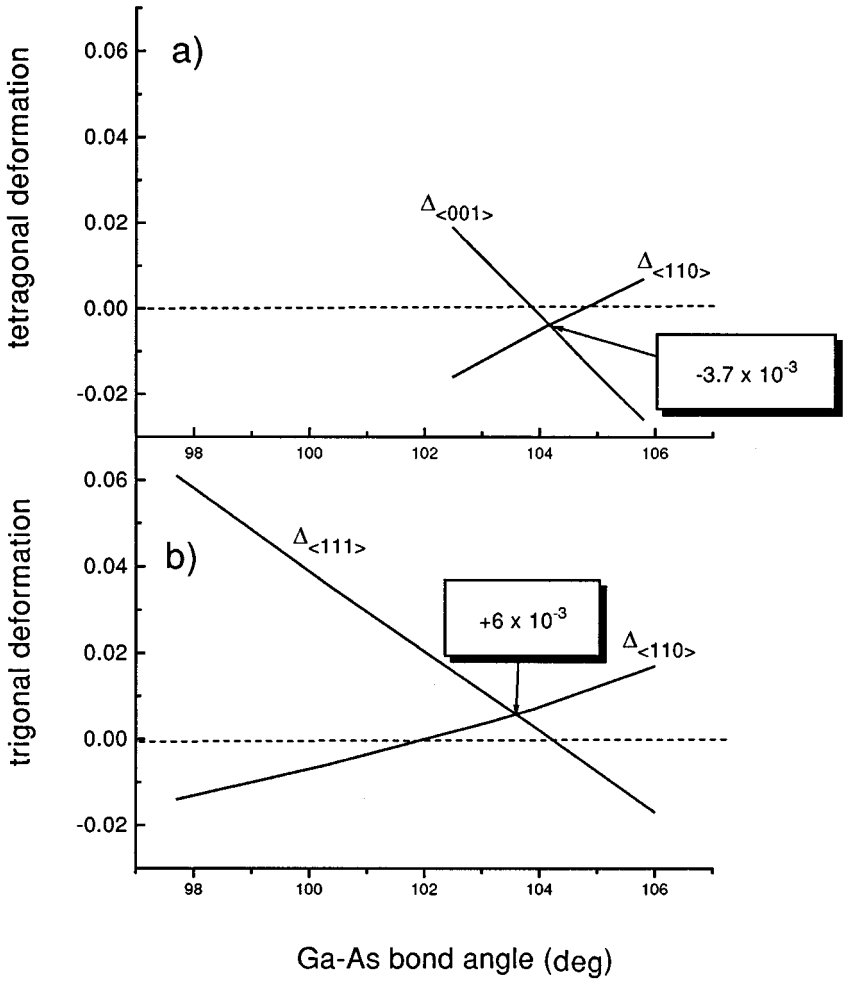

FIG. 3. Lattice deformation resulting from the formation of (a) CuAu and (b) CuPt $InGaAs_2$ structures on an InP substrate plotted as a function of the GaAs bond angle.

in the growth direction has been attributed to contrast compensation for the [111] and [111] directions. The differences in local deformations produced by different elementary tetrahedrons account for the corresponding TEM contrast and fine-scale modulation. Regions of the alloy in which the [100] and [010] strain modulation is observed contain an excess of appropriately oriented In_2Ga_2As tetrahedrons. An excess of $InGa_3As/In_3GaAs$ tetrahedrons results in modulation in the [111] and [111] directions. The SRO thus produces anticlustering. We conclude that the phase-separation effects occur in $In_{0.53}Ga_{0.47}As$ not only due to alloy composition fluctuations but also due to the SRO. This SRO phase separation is naturally connected with the observed four-mode behavior of optical phonons.

The SRO can be thought of as an order-disorder transition of the perfectly ordered structure. Thus the lattice vibrations of the SRO phase can be analyzed using phonon dispersion curves of perfectly ordered compounds. The simplest $InGaAs_2$ ordered structures giving {001} and {111} deformations that are lattice matched to InP are the CuAu- and CuPt-type structures (see Fig. 2). The tetragonal CuAu structure has the space group D_{2d}^5 and corresponds to a {001}-$(InAs)_1(GaAs)_1$ monolayer superlattice (MSL). It consists of In_2Ga_2As tetrahedrons. The rhombohedral CuPt structure has the space group C_{3v}^5 and corresponds to a {111}-$(InAs)_1(GaAs)_1$ MSL. It consists of $InGa_3As$ and In_3GaAs tetrahedrons. In Fig. 3 we plot the tetragonal and trigonal distortions as a function of the Ga-As bond angle, which are calculated assuming bulk GaAs and InAs bond lengths for these two structures. The CuAu-type structure produces smaller deformations and thus is favored. The minimum deformation corresponds to dilation, i.e., the volume of the unit cell is smaller than that of zinc-blende InP. This structure can have an excess of In (a larger atom) on Ga sites for strain compensation. On the other hand, the CuPt-type structure is compressed (higher volume of unit cell) to produce a minimum deformation. It can also accommodate strain produced by the CuAu structure, as well as having an excess of Ga on In sites. These two structures can thus coexist in epitaxial $In_{0.53}Ga_{0.47}As$ and can determine the type of SRO of *A* and *B* phases. We identify phase *A* as having predominantly CuPt-type SRO, and phase *B* as having mostly CuAu-type SRO.

The spatial and directional phonon dispersion curves of CuAu and CuPt $InGaAs_2$ structures are presented in Fig. 4. The calculations were performed using a valence overlap shell model with the parameters of bulk GaAs and InAs obtained from fitting neutron scattering data.[40,41] The bond angles correspond to deformations indicated in Fig. 3. The [001] off-axis directions correspond to the wave vectors of the two types of ordered structures, excited in Raman backscattering geometry. The frequencies of LO components of lattice vibrations of the alloy are indicated by arrows in Fig. 4. Each of the ordered phases has four atoms in the primitive cell and thus nine optical modes. For both structures there

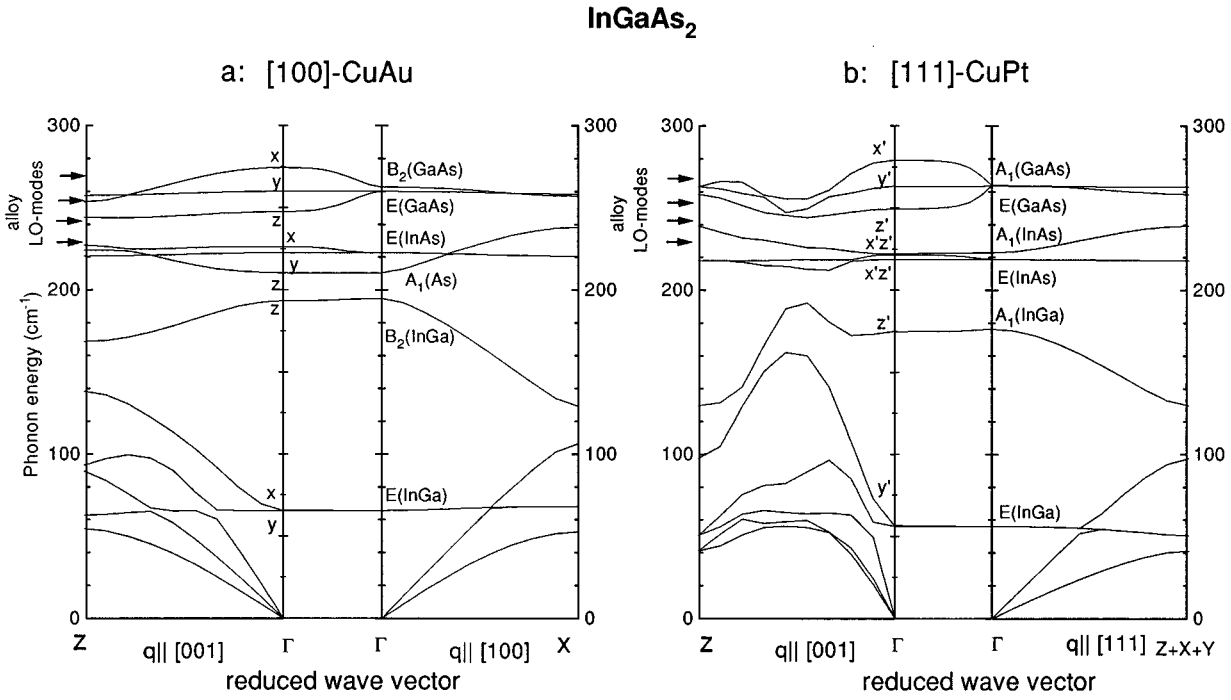

FIG. 4. Spatial and directional phonon dispersion curves of (a) [100]-CuAu and (b) [111]-CuPt structures. The zone center polarizations are indicated for the Γ-Z direction. For the CuPt structure the polarization directions, labeled z',x',y' are parallel to [111], [110], and [112] crystallographic directions.

are three distinct phonon zones—one acoustic, in the frequency range 0–190 cm^{-1}, and two optical, in the frequency range of 210–240 cm^{-1} (InAs type), and 240–275 cm^{-1} (GaAs-type). The acoustic zone includes low-frequency optical modes, denoted as InGa, which can be treated as folded zinc-blende acoustic phonons. The frequencies of the measured optical phonons of the alloy fall in different frequency regions of the corresponding calculated optical zones.

Figure 4 shows that the frequencies of polar optical zone center phonons and spatial dispersion along the crystal axis are very close in these two structures. This is expected since in our calculations we use the same set of parameters for both structures and because, for both structures, the phonon frequencies for the wave vector parallel to the crystal axis are only weakly dependent on the short-range force anisotropy. In the CuAu structure the InAs-type A_1 phonon is nonpolar. It corresponds to the antiphase displacement of two basis As atoms in a unit cell, which do not induce a dipole moment. Due to the absence of contributions of long-range forces, the zone center frequency of this phonon is considerably lower than that of a corresponding InAs-type polar A_1 phonon in the CuPt structure.

The main difference in the dispersion curves is seen for the [001] off-axis phonons [Γ-Z part of the dispersion curves in Figs. 4(a) and 4(b)] with the near zone boundary wave vectors. For these phonons, the amplitude of the atom displacements in neighboring cells is considerably different and the contribution of short-range force anisotropy becomes important. It is expected that these forces are responsible for phonon frequencies of the SRO clusters.

Figures 4(a) and 4(b) show that near the Γ-Z zone boundary, the CuPt structure exhibits higher frequencies for GaAs- and InAs-type phonons than for those of the CuAu structure. For the CuPt structure, the frequencies of the Γ-Z near zone boundary GaAs- and InAs-type phonons are 266–264 and 235–241 cm^{-1}, respectively. These values are in good agreement with the values 268 and 242 cm^{-1} measured for the Aj LO phonons in RS of $In_{0.53}Ga_{0.47}As$. For the CuAu structure, the frequencies of the Γ-Z near zone boundary GaAs- and InAs-type phonons are, respectively, 258–254 and 228–225 cm^{-1}. These are close to the values of 255 and 230 cm^{-1} measured for the Bj LO phonons. Thus our calculations and analysis of the phonon dispersion of perfectly ordered $InGaAs_2$ structures show that the Aj-type phonons are the polar optical modes of the CuPt SRO phase, while the Bj-type phonons are the equivalents in the CuAu SRO phase. This supports the statement that the four-mode behavior of the $In_{0.53}Ga_{0.47}As$ optical phonons originates from the CuAu and CuPt SRO phase separation.

In conclusion, we have carried out an experimental and theoretical investigation of the Raman PPM line shape in p-type $In_{0.53}Ga_{0.47}As$ and have shown that its optical phonons exhibit four-mode behavior. We demonstrate that the observed four-mode behavior of optical phonons in $In_{0.53}Ga_{0.47}As$ can be explained by SRO phase-separation effects. Our results illustrate the high sensitivity of lattice vibrations to the specific microstructure features in the semiconductor alloys and show excellent consistency between the vibrational spectra and structure data provided by transmission electron microscopy.

ACKNOWLEDGMENTS

Work at Texas Tech University was supported by Office of Naval Research (N0014-93-0003) and the Maddox Foundation Office of Naval Research.

[1] B. B. Varga, Phys. Rev. **137**, A1896 (1965).
[2] R. Boneville, Phys. Rev. B **24**, 1987 (1981).
[3] A. Mooradian and A. L. McWorter, Phys. Rev. Lett. **19**, 849 (1967).
[4] G. Abstreiter, M. Cardona, and A. Pinzuc, in *Light Scattering in Solids IV*, edited by M. Cardona and G. Guntherodt, Topics of Applied Physics Vol. 54 (Springer, Berlin, 1984).
[5] R. Boneville, Phys. Rev. B **29**, 907 (1984).
[6] A. Zunger and S. Mahajan, in *Handbook on Semiconductors*, Vol. 3 (Elsevier, Amsterdam, 1994).
[7] A. M. Mintairov, D. M. Mazurenko, M. A. Sinitsin, and B. S. Yavich, Semicond. **28**, 866 (1994).
[8] A. M. Mintairov, T. S. Babushkina, B. N. Zvonkov, I. G. Malkina, and Yu. N. Safianov, Solid State Physics **37**, 50 (1995).
[9] T. Yuasa, S. Naritsuku, M. Mannoh, K. Shinozaki, K. Ymanake, Y. Nomura, and M. Mihara, Appl. Phys. Lett. **46**, 176 (1985).
[10] T. Yuasa, S. Naritsuku, M. Mannoh, K. Shinozaki, K. Ymanake, Y. Nomura, M. Mihara, and M. Ishii, Phys. Rev. B **33**, 1222 (1986).
[11] D. Kirillov, Y. Chai, C. Webb, and G. Davis, J. Appl. Phys. **59**, 231 (1985).
[12] R. D. Becker, P. F. Leuhrmann, and D. W. Langer, Appl. Phys. Lett. **47**, 513 (1985).
[13] A. M. Mintairov, K. E. Smekalin, V. M. Ustinov, and V. P. Khvostikov, Fiz. Tekh. Poluprovodn. **26**, 610 (1992) [Sov. Phys. Semicond. **26**, 347 (1992)].
[14] A. M. Mintairov, K. E. Smekalin, V. M. Ustinov, and V. P. Khvostikov, Fiz. Tekh. Poluprovodn. **24**, 1539 (1990) [Sov. Phys. Semicond. **24**, 962 (1990)].
[15] T. Yuasa and M. Ishii, Phys. Rev. B **15**, 3962 (1987).
[16] A. M. Mintairov and D. M. Mazurenko, Int. J. Electron. **77**, 303 (1994).
[17] M. Qi, M. Konagui, and K. Takahashi, J. Appl. Phys. **78**, 7265 (1995).
[18] K. Sinha, A. Mascarenhas, Sarah R. Kurtz, and J. M. Olson, J. Appl. Phys. **78**, 2515 (1995).
[19] G. P. Agrawal and N. K. Dutta, *Semiconductor Lasers* (Van Nostrand, New York, 1993).
[20] T. L. McDevit, S. Mahajan, D. E. Laughlin, W. A. Bonner, and V. G. Keramidas, Phys. Rev. B **45**, 6614 (1992).
[21] T. P. Pearsal, R. Charles, and J. C. Portal, Appl. Phys. Lett. **42**, 436 (1983).
[22] K. Kakimoto and T. Katoda, Appl. Phys. Lett. **40**, 826 (1982).
[23] K. Kakimoto and T. Katoda, Jpn. J. Appl. Phys. **24**, 1022 (1985).
[24] S. Emura, S. Gonda, Y. Matsui, and H. Hayashi, Phys. Rev. B **38**, 3280 (1988).
[25] Z. C. Feng, A. A. Allerman, P. A. Barnes, and S. Perkowitz, Appl. Phys. Lett. **60**, 1848 (1992).
[26] J. P. Estrera, P. D. Stevens, R. Glosser, W. M. Duncan, Y. C. Kao, H. Y. Liu, and E. A. Beam III, Appl. Phys. Lett. **61**, 1927 (1992).
[27] S. Yamazaki, A. Ushirokava, and T. Katoda, J. Appl. Phys. **51**, 3722 (1980).
[28] M. H. Brodsky and G. Lucovski, Phys. Rev. Lett. **21**, 990 (1968).
[29] A. S. Barker, Jr. and A. J. Sievers, Rev. Mod. Phys. **47**, S1 (1975).
[30] M. B. Panish and H. Temkin, *Gas Source Molecular Beam Epitaxy* (Springer-Verlag, Berlin, 1993).
[31] M. V. Klein, B. N. Ganguly, and P. J. Colwell, Phys. Rev. B **6**, 2380 (1972).
[32] D. T. Hon and W. L. Faust, Appl. Phys. **1**, 241 (1973).
[33] *Semiconductors. Physics of Group IV Elements and III-V Compounds*, edited by K.-H. Hellwege and O. Madelung, Landolt-Börnstein, New Series, Group III, Vol. 17, Pt. a (Springer, Berlin, 1982).
[34] A. M. Mintairov, V. P. Khvostikov, V. R. Larionov, E. V. Paleeva, and S. V. Sorokina, 1994 IEEE First World Conference on Photovoltaic Energy Conversion, Record of the Twenty-Fourth IEEE Photovoltaic Specialists Conference - 1994, Vol. II, 1803.
[35] U. Nowark, W. Richter, and G. Sachs, Phys. Status Solidi B **108**, 131 (1981).
[36] W. A. Harrison, *Electronic Structure and Properties of Solids* (Freedman, New York, 1980).
[37] A. Anastassiadou, Y. S. Raptis, and E. Anastassakis, J. Appl. Phys. **60**, 2924 (1986).
[38] H. W. Verleur and A. S. Barker, Jr., Phys. Rev. **149**, 715 (1966).
[39] J. C. M. Mikkelson, Jr. and J. B. Boyce, Phys. Rev. Lett. **49**, 1412 (1982).
[40] K. Kunc and B. Bilz, Solid State Commun. **19**, 1027 (1976).
[41] P. H. Borcherds and K. Kunc, J. Phys. C **11**, 4145 (1977).